# AB INITIO STUDIES OF DISSOCIATIVE RECOMBINATION

Steven L. Guberman
Institute for Scientific Research
33 Bedford St., Suite 19A
Lexington, MA 02173

## ABSTRACT

Quantum chemical calculations of the dissociative recombination of $O_2^+$ and $N_2^+$ are reported. An approach for calculating autoionization widths from high principal quantum number Rydberg states is summarized and an example is presented for the lowest $^3\Pi_g$ dissociative state of $O_2$. For $O_2^+$, the $^1\Sigma_u^+$ state is the sole source of $O(^1S)$ from the lowest 10 vibrational levels of the ion. For $O(^1D)$, the $B^3\Sigma_u^-$, $^1\Sigma_u^+$, and $1\,^1\Delta_u$ states are the sources of $O(^1D)$ from the lowest three vibrational levels. Rate coefficients for generating $O(^1S)$ and $O(^1D)$ at ionospheric temperatures are reported. For $N_2^+$, states of $^3\Pi_u$, $^1\Sigma_g^+$ and $^3\Delta_g$ symmetries intersect the ion at the v=0 level. The configurational structure of these states indicates that the $^3\Pi_u$ states are likely to be the most important routes for dissociative recombination from v=0.

## 1. INTRODUCTION

Interest in dissociative recombination (DR) first arose out of the need to understand the properties of the Earth's ionosphere.[1],[2] Initial attention focused on the DR of $O_2^+$, $N_2^+$ and $NO^+$. While there has been much progress in the measurement of the total DR rate coefficients of these ions, the dependence of the quantum yield of excited and ground state atoms upon the electron temperature and ion vibrational level is only currently being unraveled. Impediments to experimental progress have included the difficulty of generating ions in specific vibrational levels and simultaneously identifying the atomic products.

Nevertheless there has been recent progress toward this goal.[3],[4],[5] An alternative theoretical approach based on spectroscopic identification of the potential curves which provide routes for DR is difficult since these states often do not have dipole allowed transitions from the ground state. Furthermore, electron capture occurs at high energies on the repulsive wall, well above the dissociation asymptote and out of range of the RKR approach. Additional difficulties include the paucity of information on electron capture widths although progress has been made in spectroscopic analysis of Rydberg-valence interactions[6],[7],[8],[9] from which widths can be derived.

Here, I review recent theoretical ab initio results obtained in this laboratory for the DR of $O_2^+$ and describe some preliminary results on the DR of $N_2^+$. For $O_2^+$, potential curves, electron capture widths and rate constants have been obtained for generating $^1S$ and $^1D$ atoms, the upper states of the green and red lines respectively. For $N_2^+$, potential curves for DR of the v=0 ion level have been computed.

## 2. WAVE FUNCTIONS

The wave functions calculated here are based on orbitals determined in either multiconfiguration or complete active space self consistent field (MCSCF or CASSCF) calculations. Each of the orbitals, $\phi_j$, is expanded in a large set of Gaussian basis functions, $\chi_i$,

$$\phi_j = \sum_i c_{j,i} \chi_i \qquad (1)$$

Some of the $\chi_i$ are individual Gaussian primitives[10] while others are fixed combinations (contractions) of Gaussian basis functions determined from atomic calculations.[11] The orbitals are used to construct large scale configuration interaction (CI) wave functions containing many configurations, each of which describes a possible distribution of the electrons in the molecular orbitals for a particular state symmetry. For example, for the $^1\Sigma_g^+$ ground state of $N_2$, the most important configuration near the equilibrium separation is:

$$(1\sigma_g)^2(1\sigma_u)^2(2\sigma_g)^2(2\sigma_u)^2(3\sigma_g)^2(1\pi_u)^4 \qquad (2)$$

The $1\sigma$ and $2\sigma$ orbitals are mostly N atom 1s and 2s orbitals, respectively. The $3\sigma_g$ orbital is a bonding combination consisting mostly of the N atom 2p orbitals lying along the bond axis. The $1\pi_u$ orbitals are out of plane bond orbitals consisting mostly of the N 2p orbitals that are perpendicular to the bond axis. Each configuration can have one or more spin couplings (referred to below as terms) for a given total spin symmetry. A wave function is constructed consisting of a superposition of many terms, $\Phi_i$, each of which has the same total spin and spatial symmetry,

$$\psi_j = \sum_{i=1}^{N} C_{j,i}\, \Phi_i. \qquad (3)$$

In the CASSCF[12] approach a set of active orbitals is defined and N(CASSCF) terms are generated in (3) by taking all possible excitations of the electrons within this set while restricting each term to have the total spin and spatial symmetry of interest. Both the $c_{j,i}$ and the $C_{j,i}$ are determined by variationally optimizing the total energy of $\psi_j$. The MCSCF approach is identical except that usually a subset of the full active space is used. Since the orbitals are expanded in large basis sets, $\chi_i$, the number of orbitals used in the CASSCF is only a subset of the orbitals that can be formed from the basis set. The CI wave functions are constructed by exciting electrons out of a small set of reference configurations into the remaining (virtual) orbitals. The reference configurations often consist of all the configurations needed to properly dissociate that particular state to the proper separated atoms limit. This approach leads to wave functions that are not biased to favor particular internuclear distances. Some of the wave functions reported here for $N_2$ include the $2\sigma$ orbitals in the active space and use the entire CASSCF wave function as a reference set. Taking at most one or two electrons from each of the reference configurations and promoting them to the virtual and other valence orbitals leads to a singles and doubles CI denoted CISD. The CI wave functions are expanded over the CASSCF orbitals and have the form of (3) with

N(CI)>>N(CASSCF). Some of calculations used here employ large scale wave functions having more than 100,000 terms with the CI coefficients determined by direct CI techniques.[13] Calculations have recently been completed on several states of $N_2$ and $O_2$ which provide examples of the sort of accuracy which can be expected with these techniques. For the ground state of $N_2$, 14 reference configurations (needed to properly dissociate the ground state to $^4S$ atoms) are used in the CI with a basis set consisting of 6s,3p,2d and 1f type contracted Gaussians leading to a CI wave function having 176,536 terms. The calculated (experimental[14]) spectroscopic constants are 2340.57(2356.56$cm^{-1}$) for $\omega_e$, 14.27(14.3244$cm^{-1}$) for $\omega_e x_e$, and 2.0856(2.074347$a_o$) for the equilibrium distance, $R_e$. Similar calculations on the ground state of $O_2$ using a basis set of the same size leads to a 228,036 term wave function. The calculated (experimental[15]) results are 1565.47(1580.19) for $\omega_e$, 10.93(11.98$cm^{-1}$) for $\omega_e x_e$, and 2.2999(2.2819$a_o$) for $R_e$. For $O_2$, a series of vertical excitation energies have been calculated. The calculated (experimentally derived) results are 5.8982(5.90±0.05eV) for $^1\Sigma_u^-$, 6.1318(6.11±0.05eV) for $^3\Delta_u$,6.2766(6.19±0.05eV) for $^3\Sigma_u^+$, and 8.66(8.61±0.05eV[16]) for $^3\Sigma_u^-$. All the experimental energies are derived from Ref.15 (except for $^3\Sigma_u^-$ by extending the RKR results with an ab initio repulsive wall.

Recent results have been obtained for $N_2$ using a [4s,3p,2d,1f] contracted Gaussian basis set and a CISD reference set consisting of the CASSCF configurations with $2\sigma$ in the active space. For the $C^3\Pi_u$ state the calculated (experimental)[14] results are 11.01(11.05eV) for $T_e$, 1986(2047$cm^{-1}$) for $\omega_e$, 25.05(28.44$cm^{-1}$) for $\omega_e x_e$, and 2.1932(2.1707$a_o$) for $R_e$. For the $w^1\Delta_u$ state the results are 8.83(8.84eV) for $T_e$, 1532(1559$cm^{-1}$) for $\omega_e$, 11.67(12.01$cm^{-1}$) for $\omega_e x_e$, and 2.4192(2.3977$a_o$) for $R_e$. The highly accurate values of the excitation energies and the other spectroscopic constants give us confidence that these repulsive curves will be located quite accurately relative to the ion potential curve.

## 3. POTENTIAL CURVES FOR $O_2$

Potential curves describing DR in $O_2$ and based on a [3s,2p,1d]

contracted Gaussian basis set and first order CI wave functions have been described previously.[17] These calculations showed that the $^1\Sigma_u^+$ state is the only state that can generate $O(^1S)$ from the low vibrational levels. It crosses the ion between the outer turning points of the v=1 and v=2 vibrational levels and dissociates to the $^1D + ^1S$ asymptote. The next accessible state is $5^3\Pi_g$ which crosses the outer turning point of v=10. Among the states dissociating to $O(^1S)$ there are three routes which cross the $a^4\Pi_u$ metastable state between the turning points for v=0. These routes with their dissociation limits shown in parentheses are $5^3\Pi_g(^3P + ^1S)$, $5^3\Pi_u(^3P + ^1S)$, and $4^1\Pi_g(^1D + ^1S)$. Because of its spin symmetry, the $4^1\Pi_g$ state will have only a small DR rate coefficient from the metastable state. The remaining two states can lead to hot O atoms, each with 3.4eV kinetic energy. Future experiments designed to measure the $^1S$ quantum yield must be careful to be certain that no $a^4\Pi_u$ $O_2^+$ is generated which would interfere with the determination of the $^1S$ generated from the ion ground state.

For generating $O(^1D)$, in addition to the $^1\Sigma_u^+$ state, the $B^3\Sigma_u^-$ state crosses the ion near the inner turning point of v=0 and leads to $^3P + ^1D$ atoms. A $^1\Delta_u$ state leading to two $^1D$ atoms crosses the ion near the outer turning point of v=0. The lowest valence state of $^1\Pi_g$ symmetry crosses the ion near the inner turning point of v=0 and can lead to $^1D$ atoms via a curve crossing with the $2^1\Pi_g$ state. At higher energies, the lowest $^3\Pi_g$ state crosses the ion near the inner turning point of the v=3 ion level and can lead to $^1D$ atoms via an avoided crossing with the $2^3\Pi_g$ state. The next accessible states for $^1D$ production are $2^3\Sigma_g^-(^1D + ^3P)$, $2^3\Pi_g(^1D + ^3P)$, and $2\ ^3\Pi_u(^1D + ^3P)$ near the outer turning point of v=3, $3^3\Pi_g(^1D + ^3P)$ and $2^1\Pi_g(^1D + ^1D)$ near the outer turning point of v=4. As has been pointed out earlier[17], several of these routes are expected to have small electron capture widths.

The reader is referred to Ref. 17 for a discussion of additional routes that lead to only ground state atoms.

The important $B^3\Sigma_u^-$, $^1\Delta_u$, and $^1\Sigma_u^+$ states identified above have been the subject of larger scale calculations involving [6s,3p,2d,1f] contracted Gaussian basis sets and CI wave functions that include all single and double excitations to the virtual space.[18],[19] Second order

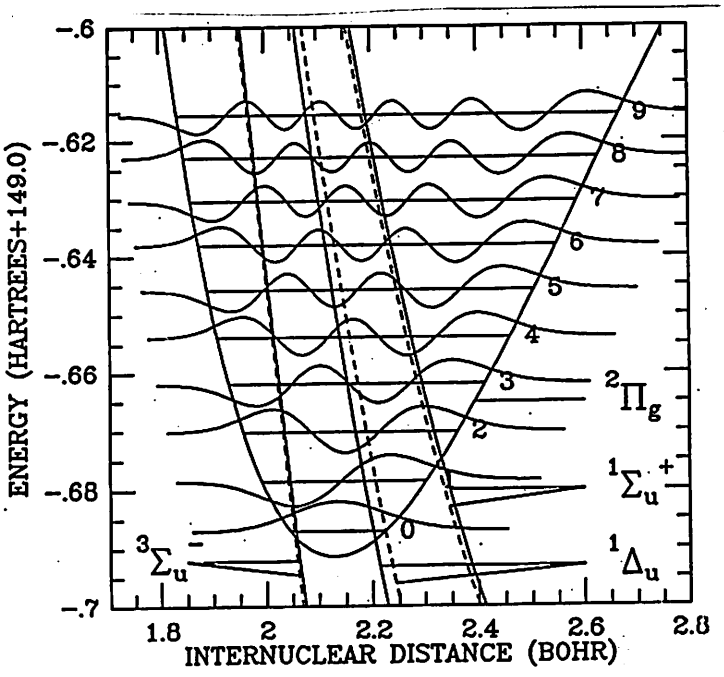


Fig. 1. Dissociative first order (dashed) and second order (solid) potentials for $O_2$ plotted with the ion potential from Ref. 15.

curves for the $\Pi_g$ states have not been obtained because of their small widths (see below). Both the earlier curves and the large scale curves are plotted in Figure 1. The ion curve is the RKR[15] curve plotted at the experimental ionization potential above the large scale calculated ground state. The ion curve has been shifted to larger R to compensate for the difference between the calculated and experimental ground state $R_e$. In order to plot the first order curves on the same figure they have been shifted to larger R to correct for the difference between the first order and second order calculated $R_e$'s. Also, the first order curves are shifted in energy so as to be plotted relative to the first order ground state. Relative to the ion, after the shift in the energy and distance coordinates, the curves are qualitatively similar. The largest difference is for $^1\Delta_u$ for which the second order curve is shifted by about $0.02a_o$ to smaller R near v=0 relative to the first order result.

## 4. ELECTRON CAPTURE WIDTHS FOR $O_2$

The DR cross section is approximately directly proportional to the

electron capture or autoionization width, $\Gamma$, a matrix element of the Hamiltonian operator, H, given by Fermi's golden rule:

$$\Gamma(R) = 2\pi\rho\left|\langle\Psi_f|H|\Psi_I^c\rangle\right|^2. \tag{4}$$

$\Psi_I^c$ is the wave function of the properly antisymmetrized product of a "free" electron in a coulomb like orbital and the wave function for the ion. $\Psi_f$ is the electronic wave function for the neutral state which describes the DR products and $\rho$ is the density of states. Rydberg orbitals with high principal quantum numbers, n, have been used to describe the coulomb like orbital. Except for the Rydberg orbital, all the orbitals in (4) are bound and have large amplitude only near the molecule. As a result, it is only important to know the amplitude of the Rydberg orbital near the molecule. The inner part of coulomb orbitals are well known to be very similar to the inner part of high Rydberg orbitals.[20] With the coulomb orbital represented as a high Rydberg orbital all the orbitals in (4) are bound and are represented in terms of Gaussian basis functions.

For $n^*>>\ell$, where $\ell$ is the angular momentum quantum number, the matrix element in (4) can be closely represented by

$$\left|\langle\Psi_f|H|\Psi_I^c\rangle\right|^2 = (1/n^{*3})k\exp(-c/n^*) \tag{5}$$

where k and c are constants determined from the calculation of the matrix elements on the left side of (5) for the highest Rydberg states. These Rydberg states are nearly hydrogenic and the energies can be represented as $E=-(1/2(n^*)^2)$ where $n^*=n-\delta$ and $\delta$ is the quantum defect. The density of states can be written as

$$\rho = 1/(E(n^*-1/2) - E(n^*+1/2)) \tag{6}$$

which can be closely represented as

$$\rho = n^{*3}\exp(-1/(2n^{*2})). \tag{7}$$

Substituting (7) and (5) into (4) gives

$$\Gamma = 2\pi k \exp(-(c/n^*)-(.5/n^{*2})). \tag{8}$$

Taking the limit of $n^* \to \infty$ gives the threshold capture width,

$$\Gamma = 2\pi k. \tag{9}$$

The Rydberg wave functions have been refined further by optimizing them in the field of an optical potential due to the $\Psi_f$ states. Feshbach projection operators[21] have been defined which partition the total space such that $\Psi = P\Psi + Q\Psi$ where $P\Psi$ contains the Rydberg states to be optimized and $Q\Psi$ are the $\Psi_f$ states described above. In the usual Feshbach projection operator formalism, an eigenvalue equation is derived for $P\Psi$ that is difficult to solve because it contains an energy-dependent optical potential. However, using partitioning techniques,[22] $P\Psi$ can easily be determined by solving the usual CI problem. Writing the total wave function as $\Psi = P\Psi + Q\Psi$, we can write the Schroedinger equation in matrix form as

$$\begin{pmatrix} H_{PP} & H_{PQ} \\ H_{QP} & H_{QQ} \end{pmatrix} \begin{pmatrix} P\Psi \\ Q\Psi \end{pmatrix} = E\,T \begin{pmatrix} P\Psi \\ Q\Psi \end{pmatrix} \tag{10}$$

where $H_{PP} = PHP$, $H_{QP} = QHP$, etc.

Multiplying the matrices in (10) leads to:

$$H_{PP}P\Psi + H_{PQ}Q\Psi = EP\Psi \tag{11}$$

and

$$H_{QP}P\Psi + H_{QQ}Q\Psi = EQ\Psi. \tag{12}$$

From Eq.(12) we have,

$$Q\Psi = H_{QP}P\Psi/(E - H_{QQ}). \tag{13}$$

Substituting Eq.(13) into Eq.(11) leads to a matrix optical potential for $P\Psi$,

$$(H_{PP} + H_{PQ}H_{QP}/(E - H_{QQ}))\ P\Psi = EP\Psi. \tag{14}$$

It is difficult to solve (14) directly for $P\Psi$ since E is on both sides of the equation. Nevertheless, $P\Psi$ can be determined by retaining the coefficients of the $P\Psi$ terms resulting from the diagonalization of the H matrix in Eq.(10). Before diagonalizing H we must project out the low energy $Q\Psi$ roots in order to prevent them from mixing into $P\Psi$. Therefore, it is necessary to first solve for the $Q\Psi$ roots by diagonalizing $H_{QQ}$. The $H_{QQ}$ portion of the H matrix in Eq.(10) is transformed to project out the physically meaningful $Q\Psi$ roots. $P\Psi$ is then determined by diagonalizing the new H matrix with the transformed $H_{QQ}$. The net effect is to provide additional correlation to the $P\Psi$ space from the nonphysical roots in the Q space. $P\Psi$'s for successive principal quantum numbers are used to represent $\Psi_I^c$ in Eq.(4). The widths obtained by this procedure are then extrapolated to the continuum as described above. The importance of the correlation added to the P space from the higher terms in Q space has been emphasized by Hazi who has described an approach similar to that used here.[23]

An application of this approach to the calculation of the widths of the B and L $^2\Pi$ states of NO has already been discussed.[24] An additional example of this approach is given in Table 1. for the $O_2$ $^3\Pi_g$ width. This is the only $O_2$ width for which there are experimentally derived matrix elements for comparison. An analysis of the released kinetic energy line width for the v=1 level of the $C^3\Pi_g$ state of $O_2$ indicates that the electronic matrix element between the C Rydberg state and the lowest valence $^3\Pi_g$ state is 0.079eV.[8] An additional determination based on the experimental line widths of the lowest 4 vibrational levels of the C state obtains a matrix element of 0.0625(+0.006,-0.004)eV.[9]

All calculations in Table 1. have been done at $R=2.2819a_o$. A [3s,2p,1d] basis set on each center was supplemented with a set a 18 diffuse s Gaussians at the midpoint and the Rydberg orbitals were determined by the Improved Virtual Orbital method.[25] The $^3\Pi_g$ valence state was described with a full valence CI consisting of 46 terms. For the C state, a valence CI on the ion ground state was coupled with the Rydberg orbital and each of the three valence virtual $\sigma_g$ orbitals leading to a 636 term CI. Using the procedure outlined above leads to

the widths shown in Table 1. Using the widths for n=8,9 gives the expression, $\Gamma = 0.00217\exp(1.39/n^*-(0.5/n^{*2}))$. The extrapolated width for $n^*\rightarrow\infty$ is 0.00217eV. This width is about two orders of magnitude smaller than the widths for the three important dissociative routes identified above. As a result, the $^3\Pi_g$ state was not included in the DR rate coefficient calculations discussed below.

Table 1. Electron-Ion Capture Widths ($\Gamma$) from $^3\Pi_g$ Rydberg States

| n | n* | $\rho(eV^{-1})$ | $\Gamma$(eV) |
|---|---|---|---|
| 9 | 7.8897 | 17.903 | 0.00257 |
| 8 | 6.8896 | 11.892 | 0.00263 |
| 7 | 5.8902 | 7.4022 | 0.00272 |
| 6 | 4.8913 | 4.2110 | 0.00285 |
| 5 | 3.8930 | 2.0972 | 0.00311 |
| 4 | 2.8959 | 0.84005 | 0.00367 |
| 3 | 1.8984 | 0.21774 | 0.00522 |

The matrix element calculated here for n=3 is 0.0617eV. Since the electronic matrix element varies with R, the experimentally derived matrix element is an averaged value. However, since the variation of the matrix element with R over the relevant range of nuclear vibrations is estimated to be less than about 10%, the results show that relatively small wave functions can yield interaction matrix elements that are in good agreement with experiment.

## 5. DR RATE COEFFICIENTS FOR $O_2$

The expression for the direct DR cross section derived by Giusti[26] has been used to calculate cross sections and rate coefficients for generation of $O(^1S)$ and $O(^1D)$ along the $^1\Sigma_u^+$, $B^3\Sigma_u^-$, and $^1\Delta_u$ diabatic potential curves described above. For DR leading to $O(^1S)$,[18] the v=2 level of the ion has the highest rate coefficient for the lowest eight vibrational levels and is a factor of 78 greater than the coefficient from v=0 at an electron temperature ($T_e$) of 300K. A comparison of the calculated rate coefficients to those deduced from atmospheric models shows that the atmospheric models apply to molecular ions which are not

in a Boltzmann distribution but which are instead significantly populated in the v>0 levels. In contrast to the situation for $O(^1S)$ generation, the total rate coefficient[19] for producing $O(^1D)$ is greatest from v=0 and is a factor of 1.9 greater than the coefficient from v=2 at $T_e$=300K. The rate coefficient for v=0 is in good agreement with those deduced from atmospheric models. The calculations show that the dominant route for producing $O(^1D)$ from v=0 is $^1\Delta_u$ and $^3\Sigma_u^-$ is the dominant route from v=1 and v=2.

Table 2. DR Rate Coefficients for Production of $O(^1S)$ for $600 \leq T_e \leq 1000$K.

| Ion Vibrational Level | Rate Coefficient($cm^3$/sec)[a] |
|---|---|
| 0 | 0.24(+.12,-.08)[-0.14] |
| 1 | 5.0(+1.2,-1.1)[-0.36] |
| 2 | 15.(+2.,-3.)[-0.50] |
| 3 | 4.8(+3.3,-2.3)[-0.77] |
| 4 | 4.9(+0.6,-1.2)[-0.32] |
| 5 | 1.2(+1.9,-0.9)[-0.90] |
| 6 | 5.1(+0.6,-1.1)[-0.56] |
| 7 | 1.4(+0.9,-0.9)[+0.06] |

a. All rate coefficients have been multiplied by $10^9$. The exponent of the temperature dependence is in square brackets. The rate coefficient for v=0 is $2.4(+1.2,-0.8)\times10^{-10}\times((T_e/800)^{-0.14})cm^3$/sec.

Since the electron temperatures in ionospheric models are near 800K, we list in Table 2. the rate coefficients for producing $O(^1S)$ for $600 \leq T_e \leq 1000$K for each of the lowest eight ion vibrational levels.

Table 3. DR Rate Coefficients for Production of $O(^1D)$ for $600 \leq T_e \leq 1000$K.

| Ion Vibrational Level | Rate Coefficient($cm^3$/sec)[a] |
|---|---|
| 0 | 1.37(+.14,-.16)[-0.51] |
| 1 | 1.09(+.12,-.14)[-0.55] |
| 2 | 0.78(+.13,-.16)[-0.41] |

a. All rate coefficients have been multiplied by $10^7$. The exponent of the temperature dependence is in square brackets. The rate coefficient for v=0 is $1.37(+.14,-.16)\times10^{-7}\times((T_e/800)^{-0.51})cm^3$/sec.

Because of the position of the intersection of the dissociative curve with the v=5 level, the coefficient from v=5 is highly sensitive to an energetic displacement of the dissociative route within its expected uncertainty (0.1eV). Table 3 has the $O(^1D)$ rate coefficients in the

same temperature range from each of the lowest three ion vibrational levels.

## 6. DISSOCIATIVE ROUTES FOR $N_2$

Preliminary results are reported here which identify the important dissociative routes for the v=0 level of the ground state of $N_2^+$. These results are based on large scale second order CI calculations using atomic natural orbital basis sets.[27] The details will be reported separately.

The dominant dissociative routes from v=0, $2^1\Sigma_g^+(^2D + {}^2D)$, $C'^3\Pi_u(^4S + {}^2P)$, $3^3\Pi_u(^2D + {}^2D)$, and $G^3\Delta_g(^4S + {}^2D)$, are shown in Fig. 2.

The dominant configuration of the $2^1\Sigma_g^+$ state is

$$....(3\sigma_g)^2(1\pi_{ux})\ (1\pi_{uy})\ (1\pi_{gx})\ (1\pi_{gy})$$

where .... denotes $(1\sigma_g)^2(1\sigma_u)^2(2\sigma_g)^2(2\sigma_u)^2$. This configuration differs by a triple excitation from the dominant configuration of the ion plus a "free" or Rydberg electron,

$$....(3\sigma_g)\ (1\pi_{ux})^2(1\pi_{uy})^2(RYD\sigma_g).$$

The matrix element of the Hamiltonian between these two configurations is zero and these dominant terms will not contribute to the electron capture width. The magnitude of the width will be determined by matrix elements between secondary terms in both states and may be small. As a result, $2^2\Sigma_g^+$ may make only a small contribution to the total DR rate coefficient from v=0.

The G state also passes through the v=0 level of the ion and dissociates to $^4S + {}^2D$ giving atoms with 1.72eV kinetic energy from v=0. The dominant configurations of this state,

$$....(3\sigma_g)^2(1\pi_{ux})\ (1\pi_{uy})\ (1\pi_{gx})^2,$$
$$....(3\sigma_g)^2(1\pi_{ux})\ (1\pi_{uy})\ (1\pi_{gy})^2,$$
$$....(3\sigma_g)^2(1\pi_{ux})^2(1\pi_{gx})\ (1\pi_{gy}),$$
$$....(3\sigma_g)^2(1\pi_{gx})^2(1\pi_{gx})\ (1\pi_{gy}),$$

differ from the ion plus a continuum electron by a triple excitation. Therefore, as for $2^2\Sigma_g^+$, the dominant configurations will not contribute

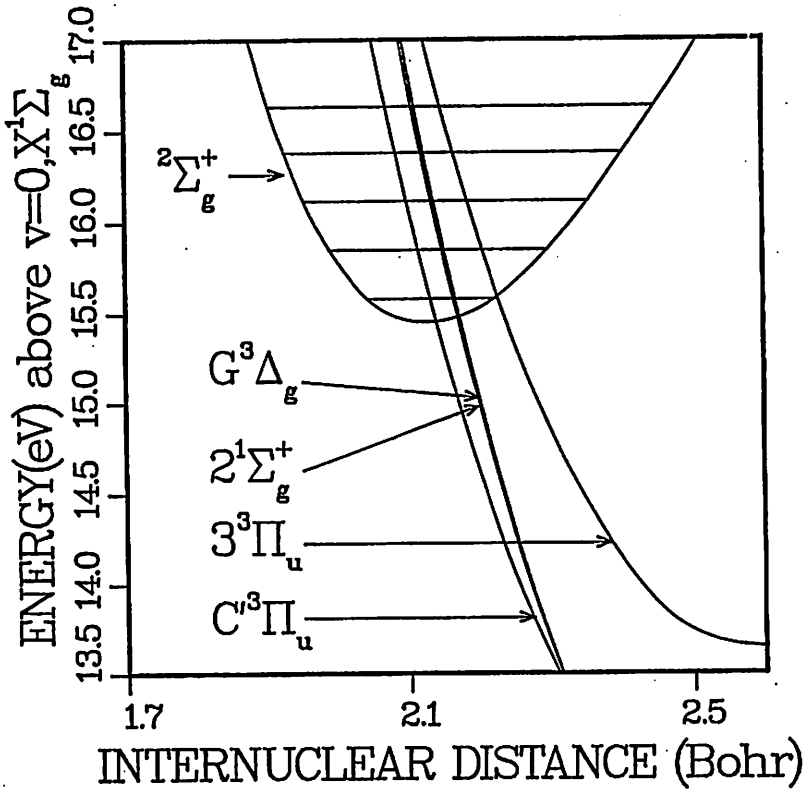


Fig. 2 Dissociative routes for the v=0 level of $N_2^+$. The ion potential is from Ref. 14.

to the width and this state is likely to have a small width and a small DR rate coefficient. This is an important conclusion for the escape of N atoms from Mars since this state and possibly the C' state (through an avoided crossing with the C state) are the only states that can supply enough kinetic energy for escape from v=0.

The primary configuration of the C' and $3^3\Pi_u$ states,

$$....(3\sigma_g)\ (1\pi_{ux})^2(1\pi_{uy})\ (1\pi_{gx})\ (1\pi_{gy}),$$

differs by a double excitation from the ion ground state plus a continuum electron. The capture width for this state may be larger than that for $2^1\Sigma_g^+$ and $G^3\Delta_g$ and it appears that these $^3\Pi_u$ states may be the dominant states for DR from v=0. The importance of the $^3\Pi_u$ states is in

good agreement with the results of Michels.[28] The C' state has an avoided crossing with the lower $C^3\Pi_u$ state which dissociates to $^4S + {}^2D$ atoms. The determination of the states of the product atoms due to initial dissociation along the C' state is currently under study.

## 7. THE ROLE OF RYDBERG STATES IN DIRECT DR OF $N_2^+$

Rydberg state potential curves having the ground state of the ion as core cannot cross the ground state of the ion and in addition have very small electron capture widths. These states are usually not important for direct DR electron capture. However, because the first excited state of $N_2^+$ is only 1.1eV above the ground state, Rydberg states having the excited state core can cross the ground state of the ion and provide routes for DR.

For $^1\Sigma_g^+$ symmetry, an $N_2$ Rydberg state can be formed by binding a $\pi_u$ Rydberg orbital to the excited $A^2\Pi_u$ state of $N_2^+$. This state will have an avoided crossing with the $2^1\Sigma_g^+$ state described above and can provide a channel for DR. A comparison to analogous states in $O_2$ indicates that the $4p\pi$ $^1\Sigma_g^+$ state having the A core will pass through the ground state of $N_2^+$ near the equilibrium separation. If the $4p\pi$ $^1\Sigma_g^+$ state should prove to have a large capture width, this route could be an important route for DR in $N_2^+$. The calculation of the potential curve for this state and the electron capture width are in progress. While the Rydberg states are diffuse, their primary configurations differ from the ion by a double excitation and they may have larger electronic widths than the $^1\Sigma_g^+$ valence state which has primary terms that differ from the ion plus a continuum electron by a triple excitation. It appears that a multistate treatment involving both the valence states and the excited core Rydberg states may be needed to calculate the cross sections for DR of $N_2^+$.

## 8. ACKNOWLEDGEMENT

This research was supported by the National Science Foundation under grant ATM-8616776 and by the National Center for Atmospheric Research

which is sponsored by the National Science Foundation. Support was also provided by NASA Grant NAGW-1404, by the Air Force Office of Scientific Research under grant AFOSR-84-0109 and by NASA Cooperative Agreement NCC 2-308.

9. REFERENCES

1. J. Kaplan, Phys. Rev. 38, 1048(1931).

2. D. R. Bates and H. S. W. Massey, Proc. Roy. Soc.(Lond.)192, 1(1947).

3. J. L. Queffelec, B. R. Rowe, M. Morlais, J. C. Gomet, and F. Vallee, Planet. Space Sci. 33, 263(1985).

4. D. Kley, G. M. Lawrence, and E. C. Stone, J. Chem. Phys. 66, 4157(1977).

5. E. C. Zipf, Planet. Space Sci. 36, 621(1988).

6. R. Galluser and K. Dressler, J. Chem. Phys. 76, 4311(1982); M. Raoult, J. Chem. Phys. 87, 4736(1987).

7. H. Lefebvre-Brion, Can. J. Phys. 47, 541(1969); D. Stahel, M. Leoni, and K. Dressler, J. Chem. Phys. 79, 2541 (1983).

8. W. J. van der Zande, W. Koot, J. Los, and J. R. Peterson, Predissociation of 3s $^{1,3}\Pi_g$ and $^{3,5}\Pi_u$ Rydberg States of $O_2$: Mechanisms and Pathways, this volume.

9. R. Friedman, private communication.

10. S. Huzinaga, J. Chem. Phys. 42, 1293(1965).

11. T. H. Dunning, Jr., J. Chem. Phys. 55, 716(1971).

12. P. Siegbahn, A. Heiberg, B. Roos, and B. Levy, Phys. Scr. 21, 323 (1980); P. E. M. Siegbahn, J. Almhof, A. Heiberg, and B.O. Roos, J. Chem. Phys. 74, 2384 (1981).

13. P. E. M. Siegbahn, J. Chem. Phys. 72, 1647(1980).

14. A. Lofthus and P. H. Krupenie, J. Phys. Chem. Ref. Data 6, 113(1977).

15. P. H. Krupenie, J. Phys. Chem. Ref. Data,1, 423(1972).

16. A. C. Allison, S. L. Guberman, and A. Dalgarno, J. Geophys. Res. in press,(1986).

17. S. L. Guberman, Potential Energy Curves for Dissociative Recombination, in Physics of Ion-Ion and Electron-Ion Collisions ed. by F. Brouillard (Plenum, New York, 1983) pp. 167-200.

18. S. L. Guberman, Nature 327, 408 (1987).

19. S. L. Guberman, Planet. Space Sci. 36, 47 (1988).

20. M. J. Seaton, Rep. Prog. Phys. 46, 167(1983).

21. H. Feshbach, Ann. Phys. (N. Y.) 5, 357(1958).

22. P. O. Lowdin, in Perturbation Theory and Its Application in Quantum Mechanics, ed. by C. H. Wilcox (John Wiley and Sons, N. Y., 1966), p.255; P. O. Lowdin, Advan. Chem. Phys. 2, 207 (1959); P. O. Lowdin, J. Math. Phys. 3, 969 (1962).

23. A. U. Hazi, Molecular Resonance Phenomena, in Electron-Atom and Electron-Molecule Collisions, ed. by J. Hinze,(Plenum Press, New York, 1983), p.103.

24. S. L. Guberman, Theoretical Studies of Dissociative Recombination, in Thermophysical Aspects of Re-entry Flows, ed. by J. N. Moss and C. D. Scott, (American Institute of Aeronautics and Astronautics, New York, 1986) pp.225-242.

25. W. J. Hunt and W. A. Goddard III, Chem. Phys. Lett. 6, 414(1969).

26. A. Giusti, J. Phys. B 13, 3867 (1980).

27. J. Almlof and P. R. Taylor, J. Chem. Phys. 86, 4070 (1987).

28. H. H. Michels, Electronic Structure of Excited States of Selected Atmospheric Systems, in The Excited State in Chemical Physics, ed. by J. M. McGowan (Wiley, New York, 1981), Vol 2; H. H. Michels, Abstracts of the Third Int. Conference on Atomic Physics, 173 (1972).